Experimental study on thickness-related electrical characteristics in organic/metal-nanocluster/organic systems

Seungmoon Pyo,[a] Liping Ma,[b] Jun He, Qianfei Xu, and Yang Yang[c]
Department of Materials Science and Engineering, University of California, Los Angeles, California 90095

Yongli Gao
Department of Physics and Astronomy, University of Rochester, Rochester, New York, 14627

(Received 8 February 2005; accepted 20 July 2005; published online 2 September 2005)

Organic bistable devices with the trilayer structure, organic/metal-nanocluster/organic, interposed between two electrodes have been systematically studied by varying the thickness of the organic layers and the metal-nanocluster layer. Devices fabricated in this fashion exhibit either electrical bistability or current step, depending on the thickness of the metal-nanocluster layer. Electrical bistable devices have been studied by fixing the metal-nanocluster layer thickness at 20 nm and changing the organic-layer thickness from 20 to 60 nm. Device injection current at the on state shows an exponential decrease with an increasing organic-layer thickness, suggesting that the electron transmission probability of the devices decreases with an increasing thickness of the organic layer. This is in agreement with theoretical calculations based on the single-band Hubbard model. The evolution of the electrical current step is observed for devices fabricated by fixing the organic-layer thickness at 50 nm and changing the metal-nanocluster layer thicknesses (2, 4, and 8 nm). The discontinuous metal-nanocluster layer is believed to lead to the observed current step. When the metal-nanocluster layer is thick enough resonant tunneling occurs between nanoclusters causing positive and negative charges to be stored on the opposite sides of the metal-nanocluster layer inducing electrical bistability. Discussions of the observed phenomena are presented. © *2005 American Institute of Physics*. [DOI: 10.1063/1.2033142]

I. INTRODUCTION

Since the 1960s, threshold switching with memory effects has been observed in a wide variety of inorganic thin films such as metal oxides[1,2] and amorphous semiconducting chalcogenide glass alloys.[3,4] In order to explain the electrical behavior of these devices several studies with inorganic semiconductor thin films as the active materials have been done.[1–4] For example, in chalcogenide glass switches and memory devices,[5] the memory effect is the result of a reversible structural change between an amorphous state, which has high electrical resistance, and a small-grain crystalline state, which is of lower resistance. Detailed studies of bistable switching in thin oxide films have also been reported.[6,7] However, there are far fewer examples of electrical switching in organic films.

The organic materials that have been studied include polymers[8–10] such as polystyrene and polyimide, charge-transfer complex materials such as metal-tetracyanoquinodimethane (TCNQ) complex,[11] blends of two materials that act as donor and acceptor,[12] and organic copper ion composites.[13] Recently, we reported the invention of a unique organic electrical bistable device (OBD) that showed reliable electrical switching and memory effects.[14–18] Unlike typical organic electronic devices, such as light-emitting diodes (LEDs) and photovoltaic (PV) cells in which the organic layer(s) is simply sandwiched between two electrodes, our device had a unique trilayer structure, organic/metal-nanocluster/organic, sandwiched between two external electrodes. In this manuscript, we systematically change the thickness of both the organic layer and the Al-nanocluster layer to study how each affects the current-voltage (*I-V*) characteristics of the OBDs in order to achieve optimal conditions for high-performance OBDs.

II. EXPERIMENT

Devices with the structure of bottom-electrode/organic/metal-nanocluster/organic/top-electrode were fabricated using vacuum thermal evaporation methods as described elsewhere.[14–17] In this article, 2-amino-4,5-imidazoledicarbonitrile (AIDCN) was used for the formation of the two organic layers with the same thickness, and aluminum (Al) was used for both the two electrodes and the metal-nanocluster layer. The deposition rates for the metal-nanocluster layer, the two organic layers, and the two electrodes were 0.3, 1, and 2 Å/s, respectively. All the depositions were carried out under the vacuum of about 2×10^{-6} torr without breaking the vacuum of the chamber. The device area is 0.25 mm^2. It should be noted that in the following, we study the organic-layer thickness effect of the device, where the thickness of the organic layer refers to each layer, not the summation of the two layers. The *I-V*

[a]Permanent address: Korea Research Institute of Chemical Technology, 100 Jang-dong, Yuseong, Daejeon, 305–600, Korea
[b]Author to whom correspondence should be addressed; electronic mail: lma@ucla.edu
[c]Author to whom correspondence should be addressed; electronic mail: yangy@ucla.edu

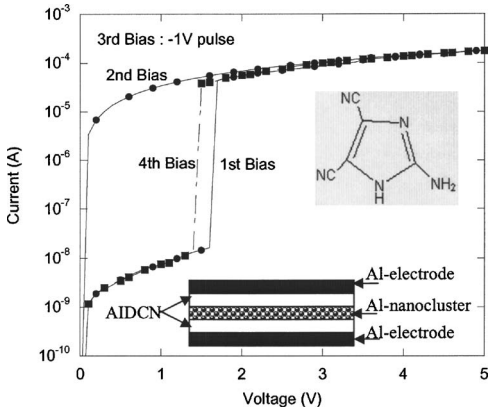

FIG. 1. The typical current-voltage characteristics of OBDs. The inset shows the device structure of an OBD and chemical structure of AIDCN.

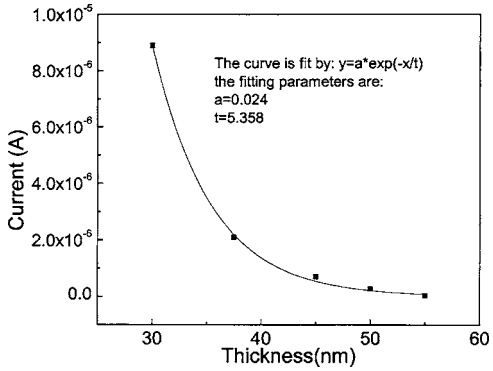

FIG. 3. Organic-layer thickness dependence of the on-state device current at 1-V bias. The solid squares are the experimental data. The curve is the exponential fit according to the results of the single-band Hubbard model (see Ref. 17). The fitting parameters have no physical meaning.

characteristics were measured by using a HP 4155B semiconductor parameter analyzer at ambient environment.

III. RESULTS AND DISCUSSION

As we reported earlier,[14–18] the typical *I-V* characteristics for OBDs are shown in Fig. 1. In addition, a schematic diagram of the device and the chemical structure of the organic active medium, AIDCN, are shown in the inset of Fig. 1 as well. During the first bias scan the device showed a sudden transition from a high impedance state (off state) to a low impedance state (on state) near 1.5 V. The current increased sharply by four orders of magnitude from 10^{-8} to 10^{-4} A. More interestingly, once the device was switched to the on state, the device remained in that state even after the applied voltage was removed, as shown in the second bias scan in Fig. 1. In addition, this transition was reversible. That is, an on state can be switched back to an off state by applying a negative bias in this case −1 V. Hence, the device was restored to the off state and another forward bias was able to repeat the switch-on behavior as shown by the fourth bias in Fig. 1. Utilizing this basic device, we first examined the dependence of the electrical characteristics of the device on the thickness of the organic layers.

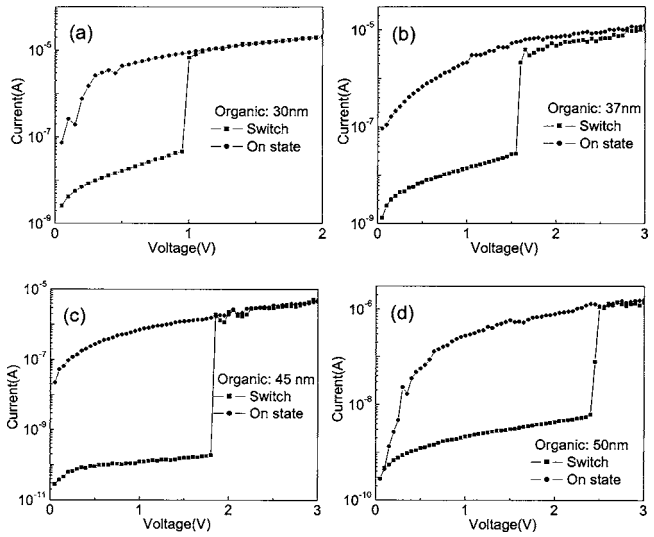

FIG. 2. *I-V* characteristics of an OBD with various organic-layer thicknesses. The Al-nanocluster layer thickness is fixed at 20 nm and the organic-layer thickness is varied as follows: (a) 30, (b) 37.5, (c) 45, and (d) 50 nm.

Devices were fabricated by changing the organic-layer thickness from 10 to 100 nm. We found that when the organic layer was too thin (10 nm) the devices showed electrical shorts. When the organic layer was too thick (100 nm) the devices showed low current injection without bistability. For an organic-layer thickness range of 20–60 nm the devices showed electrical bistability, as seen in Fig. 2. Figure 2 shows the *I-V* characteristics for devices with various organic-layer thicknesses, (a) 30, (b) 37.5, (c) 45, and (d) 50 nm.

Figure 3 shows the organic-layer thickness dependence of the on-state current for the OBDs at 1 V. It can be seen from Fig. 3 that the device current decreased exponentially with an increasing organic-layer thickness. This result was in agreement with our theoretical calculations[18] which showed that the transmission probability decays exponentially with organic-layer thickness for the device in the on state. It should be mentioned that the off-state current with a 50-nm-thick organic layer is higher than that of 45 nm, as shown in Fig. 2. We are not clear at this point; details about the mechanism governing the off-state current are under study.

In addition, the switch-on voltage shows an almost linear relationship to the organic-layer thickness for the thickness range shown in Fig. 4. This indicates that a critical electric field may more properly characterize the device than the critical voltage. It should be mentioned that the results indicated in Figs. 3 and 4 do not apply to the devices with AIDCN layer thickness outside the ranges indicated. The switch-on voltage may vary, but is generally in the range of 1–3 V.

After having explored the device characteristics by varying the organic-layer thickness we examined their behavior by fixing the organic-layer thickness at 50 nm and varying the metal-nanocluster layer thickness. It was found that the *I-V* characteristics of the devices showed an interesting evolution from current step to bistability with increasing the nanocluster-layer thickness, as seen in Fig. 5. When the nanocluster-layer thickness was below 10 nm, a current step

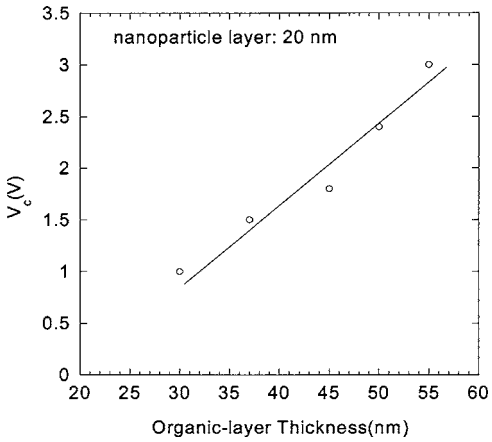

FIG. 4. Organic-layer thickness dependence of the switching voltage for OBDs with the Al-nanoclusters layer fixed at 20 nm.

was observed while threshold switching and bistability were observed for devices when the nanocluster-layer thickness was above 10 nm.

A current step was demonstrated in Figs. 5(a)–5(c). Initially, the devices showed semiconductor behavior until the applied voltage reached a critical value (V_{c1}) at which point a "constant current" was reached regardless of the increase in the applied bias. The voltage gap for the constant current range could be more than 10 V, as seen in Fig. 5(b). After the bias sweep over the second critical voltage (V_{c2}) the current rose again with increasing bias, as in Fig. 5(c). Since our devices are symmetrical, the same phenomenon was observed when the bias voltage was swept from 0 to −20 V. It can be seen from Fig. 5 that the first critical voltage shifted towards zero as the thickness of the metal nanocluster layer increased. When the thickness of the Al layer was 16 nm, a sudden current jump, as high as three orders in magnitude, was observed at a bias of about 2.2 V, as seen in Fig. 5(d), curve a. It should be mentioned that for the clear observation of both on- and off-state currents, a log scale is used for the current axis of Fig. 5(d). Here electrical bistability was demonstrated. Below the threshold voltage the device was in a low-conductance state, and above the threshold voltage the device was in a high-conductance state. The two conductance states defined the electrical bistable characteristic of the devices. The second bias ramp for the device was in the on state, as seen in Fig. 5(d) curve b, showing a memory effect. It should be noted that we have not observed a similar phenomenon with devices made using a single AIDCN film.

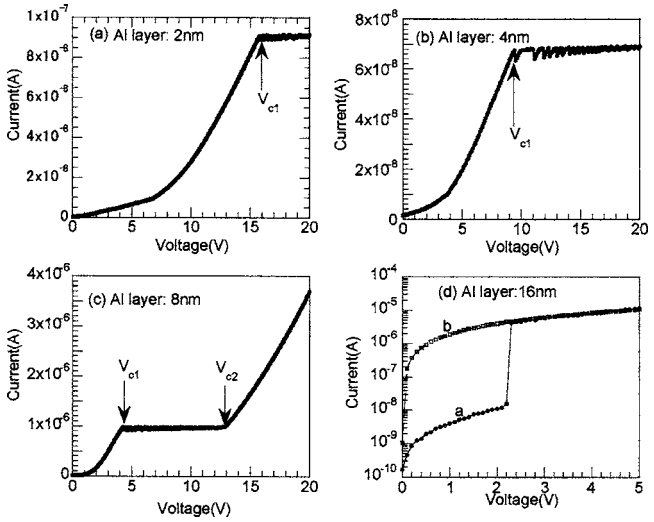

FIG. 5. The Al-nanocluster layer thickness dependence of the *I-V* characteristics of the devices. The thicknesses are (a) 2, (b) 4, (c) 8, and (d) 16 nm. The *Y* axis of (d) is in a log scale.

The current jump and bistability effect can be expected from the evolution of the current step, since the two critical voltages (V_{c1} and V_{c2}) shift in the low-voltage direction with a corresponding low current as the Al-nanocluster layer thickness increases. When the Al-nanocluster layer thickness increases to a critical value, the first critical voltage, V_{c1}, will become zero; consequently, the current of the device should be very low for biases below V_{c2}. At $V > V_{c2}$, the device shows a nearly linear *I-V* characteristic [Fig. 5(c)], which indicates that the current of the devices should have a considerable value at $V = V_{c2}$. Hence, discontinuity or threshold switching in the *I-V* curve should be expected at $V = V_{c2}$ when the thickness of the metal-nanoclusters layer is above the critical value. Indeed, we experimentally observed the current jump for the devices when the thickness of the metal layer was above a critical value, as shown in Fig. 5(d).

As previously mentioned, the devices failed to exhibit bistability when the organic-layer thickness was below 10 nm. This observation can be understood in terms of film morphology. Atomic force microscopy (AFM) was used to characterize the surface of both organic layer and the nanocluster layer. Figure 6 shows the AFM image of the surface of an AIDCN layer (here it is for the first organic layer, the second organic layer is also similar). It can be seen from Fig. 6 that the film consists of small clusters with a lateral size around 146 nm. The section line, in Fig. 6, shows that the maximum roughness of the device is about 10 nm (peak to valley). Since the film has two surfaces, electrical short may occur when the thickness of the AIDCN layer is less than 10 nm, which is in agreement with the *I-V* characteristics of the devices. Electrical bistability is observed when the thickness of the organic layer is above 20 nm. The morphology of the metal-nanocluster layer has been studied before.[17] The average nanocluster size is about 9.5 nm.

The devices with 2-, 4-, and 8-nm-thick Al layers consist of discontinuous nanoparticles, which may act as trapping centers or Coulomb islands. These Coulomb islands lead to the current steps, as observed in Figs. 5(a)–5(c). There is a considerable difference between this current step and the traditional Coulomb blockade effect. The current step for our devices is observed at room temperature, and the voltage gap for the current step is very large.[19] The current step will be discussed in detail later.

The critical thickness for the nanocluster layer, above which the devices show switching and bistability behavior, is 10 nm. Since 10 nm is almost the same size as the nanoclusters, films below 10 nm in thickness constitute the monolayer or submonolayer case, while films above the critical thickness (the nanoclusters stack vertically) become the multimonolayer case. For the multimonolayer case, resonant tunneling can occur and cause positive-negative charges to be

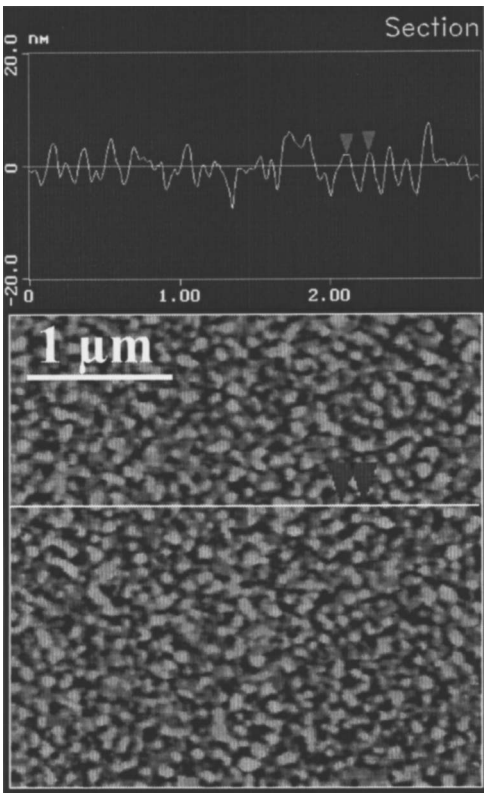

FIG. 6. A 3×3-μm^2 AFM image of the surface morphology of AIDCN film. The top curve is the cross-section line, indicating that the roughness of the surface of the film is 10 nm peak to valley. The rms roughness of the film is 2.4 nm.

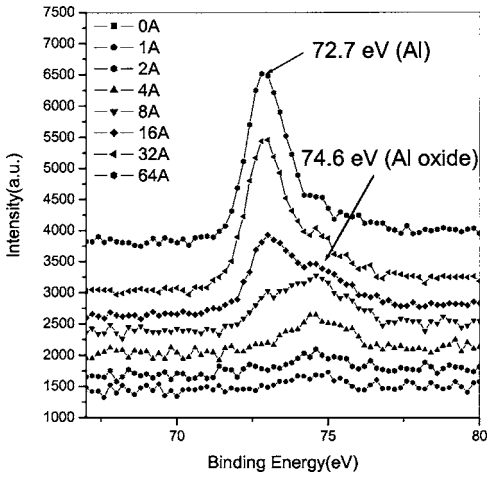

FIG. 7. The XPS spectrum of Al deposited on an AIDCN film. Al^{3+} formation is clearly seen due to the formation of the peak at 74.6 eV. At the thickness of 8 Å the coexistence of Al (72.7 eV) and oxidized Al (74.6 eV) is apparent when Al was deposited onto an AIDCN film. This experiment was carried out in vacuum at 10^{-9} torr.

stored at both sides of the nanoparticles layer.[17,18] If the nanoclusters size is further reduced, electrical bistability may be observed for devices with even thinner nanocluster layers. It should be mentioned that switching and memory effect in OBD-structured devices have also been observed by Campbell group.[20] Their devices, although they also have the organic/nanoclusters/organic structure, are different from ours. First, for their devices, the Al-nanocluster layer is only 5 nm in thickness and discontinuous. Due to this thickness and morphology, resonant tunneling within the Al-nanocluster layer may not likely happen as it does in our device.[17]

Second, their current-voltage (*I-V*) characteristics are different from ours. For their device, the on state is restored to the off state at higher voltage, and they observed a kind of negative differential resistance phenomenon, whereas for our devices, reversed bias restores the device from the on state to the off state. Therefore we believe that the mechanism for their device is different from ours.

The formation of the nanoclusters is caused, in part, by surface oxidation of the nanoclusters during deposition. This assertion is supported by both *in situ* resistance-thickness measurements and x-ray photoelectron spectra. The x-ray photoelectron spectroscopy (XPS) and *in situ* resistance measurement results indicate that the nanocluster layer is not pure metal, but instead a mixture of metal and oxidized metal that is formed during deposition. There are two potential sources of Al^{3+}: (1) oxidized Al formed by reaction with residual O_2 in the chamber, and (2) Al–AIDCN complex formed by charge transfer between the Al and AIDCN during deposition. Oxidized Al formation was clearly observed, as shown in Fig. 7 (Al^{+3}, here it may not only represent Al_2O_3, but also Al–AIDCN complex). Our OBDs were fabricated at 10^{-6} torr, with a slow deposition rate for the Al-nanocluster layer (0.3 Å/s), which may provide more chance for the Al to react with other background gases within the chamber such as oxygen and AIDCN vapor. Since AIDCN and Al were deposited within the same chamber, it is possible that a small amount of AIDCN may also evaporate because of the heating of the Al boat. In addition, the amount of AIDCN for Al-nanocluster layer formation can be controlled on purposely by codeposited Al and AIDCN for the Al-nanocluster layer formation.[14] In other XPS measurements, we also observed the Al^{3+} peak (74.6 eV) from Al (2*p*) spectrum, C (1*s*) peak shift from 286.7 to 285.1 eV, and N (1*s*) peak broadening (not shown here). This observation suggests a chemical reaction or charge transfer between Al and AIDCN,[21,22] as noted above. Al–AIDCN complex can be formed during coevaporation of Al and AIDCN for the nanocluster-layer formation.[17] Since Al is a very reactive and good electron donor, and the CN triple bond of AIDCN is a strong electron acceptor, charge transfer between Al and CN bond is likely to happen. In addition, the *in situ* resistance result for a 20-nm film, seen in Fig. 8, is $\sim$1000 Ω, which is much larger than that of a pure metallic Al thin film. As a result, we conclude that the Al-nanocluster layer of the OBDs consists of nanoclusters with an oxidized coating between the metallic cores. The oxidized coating is necessary to the formation of individual metallic Al nanoclusters. Without the oxide coating the Al nanoclusters stick together forming a smooth continuous film.

Based on our observations concerning nanocluster formation we can explain the observed *I-V* characteristics, shown in Fig. 5, as follows. Figure 9 shows the schematic structure diagram for the current-step case and the switching and memory case. When the Al-nanocluster layer is a monolayer or submonolayer, the *I-V* characteristics are controlled

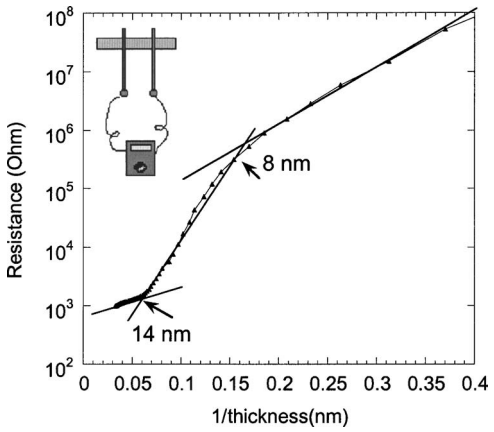

FIG. 8. The *in situ* resistance-thickness measurement for the Al-nanocluster layer (1×3 mm^2) during deposition. The insert shows the schematic diagram for the measurement.

by charge injection-trapping (*I-T*) as shown in Figs. 9(a). When the Al-nanocluster layer is a multilayer case as shown in Fig. 9(b) (more than two nanoclusters are stacked perpendicular to the in-plane film direction), the *I-V* characteristics of the devices are controlled by the resonant tunneling and charge storage (RT-CS).[17,18] The key issue for the evolution from *I-T* to RT-CS picture is the Al-nanocluster layer transition from a submonolayer to a multilayer.

For the submonolayer case as shown in Fig. 9(a), there may be some bypass that is not fully covered by the nanoclusters. We propose that the Al nanoclusters act as charge traps. The traps have an energy barrier (due to the oxide coating, the barrier width is the thickness of the coating) covering the metallic cores (trap centers). Below V_{c1} [shown in Fig. 5(c)], the applied voltage is not high enough to let the injected carriers overcome the barrier that surrounds the trap center so no charge is trapped. Current just goes through the bypass. When the applied bias is high enough ($V>V_{c1}$), some of the injected charges are able to jump into the trap centers. The trapped charges will act as Coulomb islands and show a blockade effect to further current injection. Therefore, a current step is observed, as shown in Fig. 5(a)–5(c). It should be mentioned that the trapped charges still have an opportunity to escape from the trap centers if the barrier width is not sufficiently wide. In support of this case, a current plateau can be observed at a relatively fast bias scan rate. Lower bias scan rates may allow some of the trapped charge to escape, lowering the blocking effect, consequently, leading to a current step that is not flat and has a small slope, which we have observed (not shown here) for slow scanning-bias rates. When the applied bias is large enough ($V>V_{c2}$) to fill all of the traps, further injected charges will not be trapped and they will be transported throughout the device and contribute to the measured current. Therefore, the current increases again with the bias above V_{c2}.

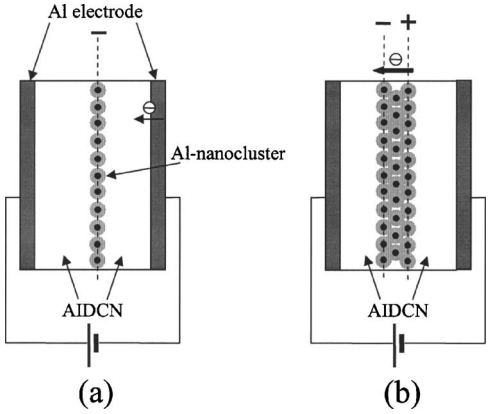

FIG. 9. (a) The schematic diagram for devices with characteristics of (a) current step and (b) electrical bistability.

For the multilayer case as shown in Fig. 9(b), the energy barrier width between adjacent Al-metallic cores is twice as thick as the single oxide coating thickness, which provides higher tunneling resistance for charge carriers. The device with structure as shown in Fig. 9(b) shows electrical bistable behavior. We have proposed a model and done theoretical calculations based on the single-band Hubbard model,[18] in order to explain this behavior. The simple explanation of the model for this bistable behavior is given as follow: at small bias, the transmission probability is small near the Fermi level if no charges are stored in the nanoclusters layer, which corresponds to the low-conductance state of the device. Above a threshold bias, the electrons within the metallic cores of Al nanoparticles will tunnel resonantly from one side to the other side, and the resulting positive-negative charges are stored at both sides of the Al-nanoparticles layer, in which case the transmission probability increases tremendously near the Fermi level, resulting in the high-conductance state. A small reverse bias may neutralize the positive-negative charges and restore the device to the off state. Recently, we did experiments to study the Al-nanocluster/AIDCN interfacial contact resistance by preparing two devices with the following structures: (1) Al/AIDCN/Al-nanocluster and (2) Al/AIDCN/Al. Each device has two interfacial contacts. The two devices have one contact that is the same, the Al/AIDCN layers (both devices were deposited together). They differ in the second contact, the AIDCN/Al and AIDCN/Al-nanocluster interfaces. It should be mentioned that the resistance of the Al-nanocluster electrode is much lower than that of the devices and can be neglected here. We measured the *I-V* characteristics of the two fresh devices, at small bias condition (read mode), and found that the resistance of the device with AIDCN/Al-nanocluster contact is about three orders in magnitude higher than that of the device with AIDCN/Al contact (not shown here). This result indicates that the Al-nanocluster/AIDCN interface generally provides a high-resistance contact, and the high-resistance state may be responsible for the off state of the OBDs. Once positive-negative charges are stored at the two sides of the Al nanoclusters, the Al-nanocluster/organic interface may turn to the low-resistance state by the easy charge injection from this interface. This process happens within a nanoseconds range, where the injected charges from the electrode may not have enough time to travel through the organic layer when a short voltage pulse is applied. In addition, for the multilayer case, the potential distribution within the device may be different from the mono or submono layer case, and the charge redistribution process within the Al-nanocluster layer happens more likely at the

small switching voltage (around 1.6 V) than the trapping process, and dominates the *I-V* characteristics of the device.

In the paper, we have discussed devices for two different cases concerning the Al-nanoclusters layer, (1) the monolayer case and (2) the multilayer case. For the monolayer case, the injected charge has the same sign as the charge trapped by the Al nanoclusters. As a result, the charged state for the monolayer case may show a higher resistance than that of the none-charge trapped state because of the Coulomb repulsive force. However, for the multilayer case, the electric field produced by the positive-negative stored charges will enhance charge injection at the Al-nanocluster/AIDCN interface. Hence, the charged state for the multilayer case shows much lower resistance than that of the noncharged state. It should be mentioned that the fresh OBDs without any bias history always show a high-resistance state initially, which corresponds to a noncharged state. The off state of the OBDs is stable and its retention time is unlimited, as we measured. On the other hand, the on-state retention time of OBDs is not as stable as the off state. This observation is also consistent with the fact that the stored charges in the Al nanoclusters have certain probability to escape from the energy wells of the Al nanoclusters and restore the device to the off state. Details about how to modify the energy barrier and increase the on-state retention are under study.

IV. CONCLUSIONS

We have fabricated devices with the nominal layer structure of organic/metal-nanocluster/organic interposed between two electrodes by a vacuum evaporation method. Aluminum and 2-amino-4,5-imidazoledicarbonitrile have been used for the metal-nanocluster layer and the two organic layers. It is found that the current-voltage characteristics of the devices at room temperature show a systematic change with the variation of the thickness of the Al-nanocluster layer when the organic-layer thickness is fixed. For the thickness below a critical value (10 nm), a current step is observed. The current step shifts toward low voltage with an increasing metal-nanocluster layer thickness. When the thickness of the Al-nanocluster layer is above 10 nm, a sudden current jump is observed at about 1–3 V. The observed evolution from current step to bistability is caused by a shift of the nanocluster layer from the submonolayer case to the multilayer case. For the submonolayer case, charge injection and trapping mechanisms dominate the current transport. For the multilayer case, resonant tunneling and charge storage dominate the device. When fixing the aluminum nanocluster-layer thickness at 20 nm, the devices with the organic-layer thickness ranging from 20 to 60 nm show electrical bistability. The current of the device shows an exponential decrease with the increase of the organic-layer thickness, which is in agreement with theoretical calculations from the single-band Hubbard model.[18]

This research is partially supported by the Air Force Office of Scientific Research (F49620-01-1-0427; program director, Dr. Charles Lee), the Office of Naval Research (N00014-01-1-0855; program director, Dr. Paul Armistead), and the National Science Foundation (ECS-0100611; program director, Dr. Usha Varshney).

[1] J. F. Gibbons and W. E. Beadle, Solid-State Electron. **7**, 785 (1964).
[2] F. Argall, Solid-State Electron. **11**, 535 (1968).
[3] J. F. Dewald, A. D. Pearson, W. R. Northover, and W. F. Peck, Jr., J. Electrochem. Soc. **109**, 243 (1962).
[4] S. R. Ovshinsky, Phys. Rev. Lett. **21**, 1450 (1968).
[5] D. Adler, M. S. Shur, M. Silver, and S. R. Ovshinsky, J. Appl. Phys. **51**, 3289 (1980).
[6] A. Beck, J. G. Bendnorz, Ch. Gerber, C. Rossel, and D. Widmer, Appl. Phys. Lett. **77**, 139 (2000).
[7] C. Rossel, G. I. Meijer, D. Bremaud, and D. Widmer, J. Appl. Phys. **90**, 2892 (2001).
[8] H. K. Henisch and W. R. Smith, Appl. Phys. Lett. **24**, 589 (1974).
[9] K. Takimoto, H. Kawade, E. Kishi, K. Yano, K. Sakai, K. Hatanaka, K. Eguchi, and T. Nakagiri, Appl. Phys. Lett. **61**, 3032 (1992).
[10] Yu. G. Kriger, N. F. Yudanov, I. K. Igumenov, and S. B. Vashchenko, J. Struct. Chem. **34**, 966 (1993).
[11] R. S. Potember and T. O. Poehler, Appl. Phys. Lett. **34**, 405 (1979).
[12] H. J. Gao, K. Sohlberg, Z. Q. Xue, H. Y. Chen, S. M. Hou, L. P. Ma, X. W. Fang, X. W. Fang, S. J. Pang, and S. J. Pennycook, Phys. Rev. Lett. **84**, 1780 (2000).
[13] L. P. Ma, Q. F. Xu, and Y. Yang, Appl. Phys. Lett. **84**, 4908 (2004).
[14] J. He, L. P. Ma, J. H. Wu, and Y. Yang, J. Appl. Phys. **97**, 064507 (2005).
[15] L. P. Ma, J. Liu, and Y. Yang, Appl. Phys. Lett. **86**, 2997 (2002).
[16] L. P. Ma, J. Liu, S. Pyo, Q. Xu, and Y. Yang, Mol. Cryst. Liq. Cryst. Sci. Technol., Sect. A **378**, 185 (2002).
[17] L. P. Ma, S. M. Pyo, J. Ouyang, Q. Xu, and Y. Yang, Appl. Phys. Lett. **82**, 1419 (2003).
[18] J. H. Wu, L. P. Ma, and Y. Yang, Phys. Rev. B **69**, 115321 (2004).
[19] T. Bergsten, T. Claeson, and P. Delsing, Appl. Phys. Lett. **78**, 1264 (2000).
[20] L. D. Bozano, B. W. Kean, V. R. Deline, J. R. Salem, and J. C. Scott, Appl. Phys. Lett. **26**, 607 (2004).
[21] C. Shen and A. Kahn, J. Appl. Phys. **90**, 6236 (2001).
[22] G. Parthasarathy, C. Shen, A. Kahn, and S. R. Forrest, J. Appl. Phys. **89**, 4986 (2001).